Classification
Physics Abstracts
61.30 ; 47.90

MARANGONI EFFECT IN NEMATIC LIQUID CRYSTALS

W. URBACH (*), F. RONDELEZ

Physique de la Matière Condensée, Collège de France, 75231 Paris Cedex 05, France

and

P. PIERANSKI, F. ROTHEN (**)

Physique des Solides (†), Bât. 510, Université de Paris Sud, 91405 Orsay Cedex, France

(*Reçu le 18 avril 1977, accepté le 24 juin 1977*)

Résumé. — On a pu mettre en évidence des écoulements hydrodynamiques induits par variation thermique de la tension superficielle dans des gouttelettes orientées de cristaux liquides nématiques. (Cet effet est connu sous le nom d'effet Marangoni dans les liquides isotropes.)

Le couplage entre l'orientation moléculaire et l'écoulement hydrodynamique provoque des distorsions de l'alignement moléculaire. On observe alors des figures optiques très particulières au microscope polarisant. On montre que l'alignement moléculaire à l'interface nématique — air, ainsi que les conditions d'ancrage, peuvent être déduits de ces observations.

Les équations hydrodynamiques du système ont été résolues et donnent des prédictions en bon accord avec les résultats expérimentaux. En particulier une simulation sur ordinateur a permis de déterminer l'orientation moléculaire en tout point de la surface libre et de reconstruire les figures optiques observées au microscope.

Abstract. — Streaming due to thermal surface tension gradients — the so-called Marangoni effect in isotropic fluids — has been observed in thin droplets of nematic liquid crystals deposited on a glass substrate.

The coupling between the molecular orientation and the hydrodynamic flow induces distortions in the molecular alignment. This results in striking optical patterns which are directly related to the distortion of the molecular alignment at the nematic-air-interface. We also demonstrate that this experiment provides a simple test to determine the anchoring conditions of the molecules at the interface.

The hydrodynamic equations have been solved and their solutions proved to be in good agreement with the experimental results. In particular a computer simulation has allowed us to describe completely the director field on the free surface and to reproduce numerically the optical patterns observed under the microscope.

1. **Introduction.** — Surface properties of liquid crystalline phase have been studied much less than bulk ones. The few existing experiments have been restricted mainly to measurements of the surface tension [1-2] and to the determination of the molecular orientation [3-5] at the free surface of a nematic liquid crystal. So far, it has been shown that :

1) Surface tension in the nematic phase decreases with temperature and has a discontinuity at the nematic to isotropic transition.

2) Orientation of the molecules at the nematic-air interface is well defined but is strongly dependent on both the liquid crystalline compound and the presence of surface-active contaminants. It is generally assumed for instance, that the angle with the free surface is $\sim 0^{o}$ for P.A.A. molecules and $\sim 15^{o}$ for M.B.A.A. molecules. Theoretical arguments based on a molecular theory of surface tension have recently been proposed by Parsons [6] to explain these observations.

In this paper, we describe a streaming experiment in nematic droplets driven by thermally induced surface tension gradients. The associated hydrodynamic flows can easily be visualized without seeding particles due to the peculiar optical properties of liquid crystals. The analysis of the molecular distortion induced by the hydrodynamic flow shows unambiguously the

(*) Permanent address : Laboratoire de Biophysique, C.H.U. Cochin, 75014 Paris.

(**) Permanent address : Institut de Physique Expérimentale de l'Université, Bâtiment des Sciences Physiques, 1015 Lausanne-Dorigny, Suisse.

(†) Laboratoire associé au C.N.R.S.

existence of a tilt angle of the M.B.A.A. molecules at the interface and we suggest the use of this method as a simple test of surface molecular alignment in liquid crystalline phases.

In section 2, we recall that streaming in liquids can be induced by thermal surface tension gradients and has indeed been observed in a number of experiments on isotropic liquids.

In section 3, we present experimental evidence that a similar effect can be found in nematic liquid crystals when a thin nematic layer is heated locally by a laser beam. We show that the viscous torque applied to the molecules by the hydrodynamic flow distorts the initial orientation and that this distortion is easily detected with polarizing optics.

In section 4, we calculate a theoretical estimate of the flow pattern and the corresponding molecular distortion. To facilitate the comparison with the experimental observations, a computer simulation of the light intensity transmitted by the sample between crossed polars is also given.

Finally in section 5, we compare the theoretical predictions with the experimental results and explain why natural convection can be neglected.

The conclusions are followed by an appendix which shows how the equations describing the equilibrium conditions have been solved.

2. **Thermal streaming in liquids.** — Surface tension at air-liquid interface is generally temperature dependent. Thus, local heating will create a gradient of temperature, which couples to the surface tension σ [1] to give a net force $f_\beta = \nabla_\beta \sigma$. This force will drive hydrodynamic flows which tend to give a new shape to the droplet in the stationary regime.

This surface tension-driven flow is known as the Marangoni effect [7]. It plays a crucial role in the original Bénard experiment on convection [8], in the recent Apollo 17 space flight experiments on thermal convection under zero gravity field [9], and in various experiments on liquids in which the surface tension is particularly small [10].

In all these experiments, the flow pattern is usually detected by visual observation of small particles suspended in the fluid, e.g. graphite or aluminium powder.

It is obvious that similar streaming due to thermal surface tension gradients should exist in liquid crystals, although this has never been demonstrated so far. The temperature dependence of the surface tension has been reported by several authors for nematic liquid crystals [1, 2]. Moreover, their peculiar optical properties in polarized light should allow for an easy observation of the flow lines without seeding. The local optic axis for these uniaxial materials is parallel to the average molecular orientation described by the director **n**. A distortion of the optic axis resulting from the coupling between the flow and the molecular orientation will be visualized as a change in the light intensity transmitted between crossed polarizers.

Our experimental observations are fully described in section 3.

3. **Experimental observations in M.B.B.A.** — 3.1 INITIAL CONFIGURATION. — A drop of nematic liquid crystal M.B.B.A. (p-methoxybenzylidene, p-n-butyl aniline) is spread on a glass substrate as a 60-200 μm thick homogeneous layer.

At the glass-nematic liquid interface, the molecular orientation of the M.B.B.A. molecules is planar and parallel to the X axis of figure 1. This is obtained by deposition under oblique incidence of a thin SiO film on the glass plate [11].

At the liquid-air interface, the molecular orientation for M.B.B.A. molecules is known to be conical, with a 15° angle relative to the surface [3] and continuously degenerate. In our set up, this degeneracy is partially removed since the molecules will stay in the XOZ plane, in order to minimize the bulk elastic free energy [12]. However, there are two equivalent configurations A and B which are indeed observed under the microscope as large domains separated by disclination lines. In the following, we shall work with A-type domains only (see Fig. 1). The sample appears black between crossed polarizers parallel and perpendicular to OX respectively.

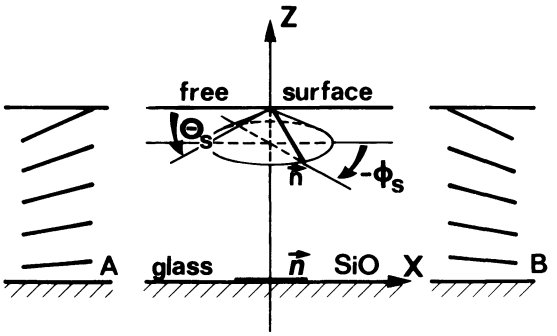

FIG. 1. — Schematic representation of the unperturbed molecular alignment throughout the sample thickness.

3.2 PRODUCTION OF THE TEMPERATURE PATTERN. — A convenient way to produce a well-defined temperature pattern is to use laser beam absorption by the sample. If necessary, the sample is made more absorbing at the laser wavelength by addition of dyes. Here we have used a He-Ne laser (Spectra Physics model 124, $\lambda = 6\,328$ Å) and a 10^{-3} concentration of nitrozo di-methyl aniline. This light-absorbing dye has a broad absorption band in the visible [13]. The laser power incident on the sample can be varied between 2 and 15 mW with neutral density filters.

(1) We will assume here that surface tension can be described by a scalar. This is justified by recent experimental evidence showing that the surface tension in nematic crystals is isotropic [1].

The determination of the temperature distribution induced by the laser heating is made by visual inspection of the boundary line separating the central isotropic region from the peripheral nematic region while the average sample temperature is varied with an electrically-heated hot plate. The shift of this isotherm is a direct measure of the temperature gradients existing at given laser power levels. For 15 mW, the temperature gradient was $\sim$ 1.7 °C/cm at a distance 0.5 mm from the hot spot for a sample thickness of 100 μm. The experiments were generally performed with smaller incident laser powers, e.g. 2 mW, and correspondingly smaller temperature gradients.

3.3 OBSERVATIONS UNDER THE MICROSCOPE. — 3.3.1 *Optical distortion.* — The nematic droplet is observed between crossed polarizers with a 5 × 10 magnifying power Leitz Orthoplan-pol microscope which gives a view field of 1 m/m diameter.

As mentioned already, the optical field is black in the absence of laser heating. When the laser beam is turned on, a characteristic pattern develops progressively around the heating point.

Figure 2 displays a typical picture. We observe a combination of dark and bright regions with a striking overall butterfly-like shape. In the bright regions, the molecular orientation has turned away from its initial direction. More precisely, a light beam, incident on the sample through the glass substrate and linearly polarized along OX, will come out of the droplet with a polarization which is still linear but has been rotated by an angle φ_s [14]. φ_s is the azimuthal angle of the molecular orientation on the free surface. Consequently, we are essentially probing the molecular orientation at the liquid-air interface. This argument is valid because the molecular distortion extends over the whole sample thickness, i.e. distances large compared to the wavelength of light. The transmitted intensity between crossed polarizers will be

$$I = I_0 \sin^2 \varphi_s .$$

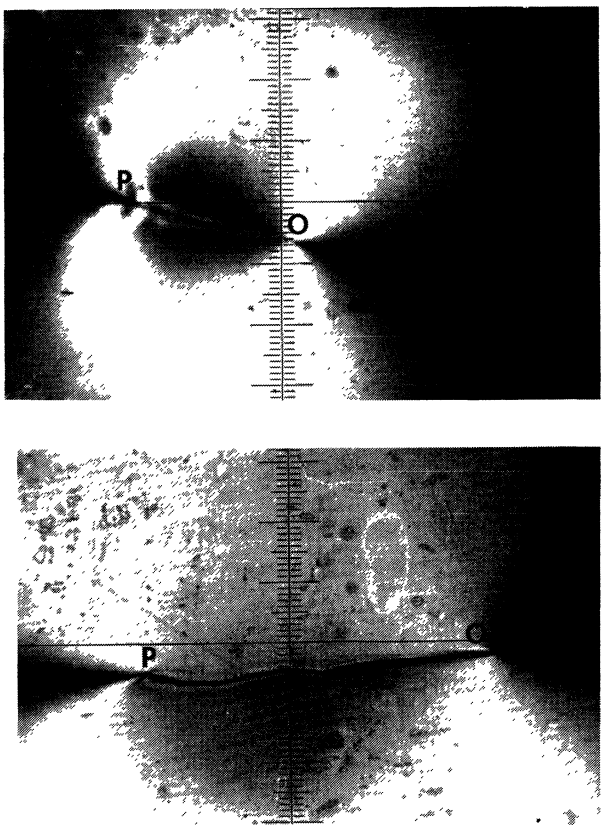

a)

b)

FIG. 2. — *a)* Optical appearance of the distortion induced by the laser heating-crossed polarizers. The hot spot (point O) is on the vertical scale, at −6 divisions (1 div = 28.6 μm). *b)* Detailed picture of the OP line.

The picture is asymmetric relative to the heating point O. In figure 2, the vector **OP** is antiparallel to the X axis for A-type domains. On the contrary, **OP** is parallel to **OX** when the experiment is performed in B-type domains.

It is also interesting to observe the relaxation of the distorted structure towards the equilibrium configuration when the laser is turned off. The optical picture annihilates progressively towards the point O, and becomes black. Then an inverted picture emerges from point O, symmetrically opposite the initial one, grows, and finally decreases towards point O and stays black definitely.

The points O and P correspond to singularities in the surface molecular alignment. Around O, which is the heating point, the alignment is degenerated and the molecules have a star-like configuration. This explains the two dark stripes parallel to the analyzer on the photograph of figure 2. The molecular configuration around the other point P is less obvious and will be fully understood only after the problem has been solved numerically in section 4. The distance r_0 between these 2 points is strongly dependent on the actual parameters of the experiment (sample thickness, heating power...) Figure 3 shows the dependence of r_0 *versus* the incident laser power. Within the experimental accuracy, we get a linear plot.

3.3.2 *Velocity field.* — Simultaneously with the formation of the optical image, we observe that the fluid of the droplet is set into motion. Floating dust

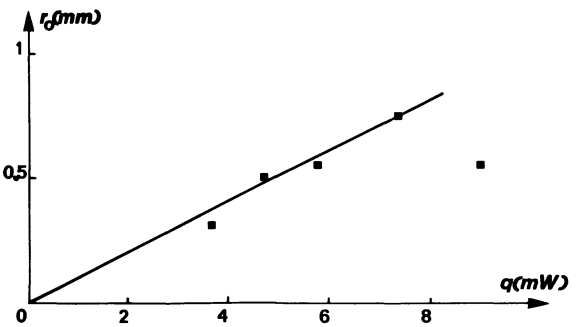

FIG. 3. — Dependence of the distance between the 2 singular points O and P on the incident power of the heating laser.

particles (typical size ~ several μm) are displaced radially from their original position.

By focusing the microscope at various depths within the droplet, it is possible to determine the velocity profile qualitatively. Near the free surface, the velocity is maximum and directed radially outwards. When approaching the bottom, the velocity decreases and eventually changes its sign.

The motion of suspended particles is clear evidence that hydrodynamic flows are associated with the distortion of the molecular alignment, itself revealed by the appearance of the butterfly-like pattern.

3.3.3 *Shape variation of the droplet.* — In order to sustain the hydrodynamic flow within the fluid in the stationary regime, the droplet has to change its initial shape. This deformation is easily observed with the naked eye as a change in the droplet optical reflectance when the laser heating is turned on. A dip is formed around the hot spot and for high enough temperature rises, a hole, free of liquid crystal, can even be observed at the center of the drop.

4. **Theory.** — In this paragraph, we will first write the equations for the temperature distribution T and the velocity field $\mathbf{V}$ induced by the Marangoni effect. We then calculate the associated distortion of the director field $\mathbf{n}$ on the free surface taking into account the restoring elastic torques due to the anchoring conditions.

Let us choose a set of cylindrical polar coordinates (Fig. 4). We take as our origin the hot point O, supposed to be situated on the glass-liquid interface (as we shall see later, the choice of a vertical position for O is unimportant). We define r and Z as the horizontal and the vertical distances measured from 0. $Z = 0$ defines the glass-nematic interface, $Z = Z_0$ the nematic-air interface in the unperturbed situation (no heating). We also introduce ψ as the polar angle whose origin is taken on the OX axis introduced above.

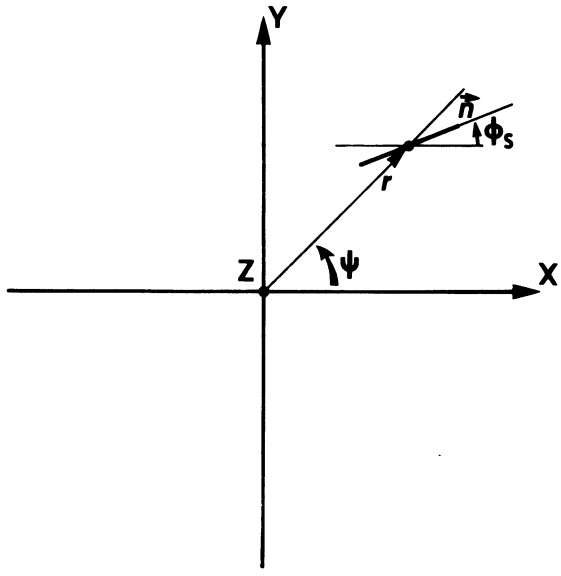

FIG. 4. — Definition of the various angles describing the director field in an horizontal plane $\tilde{z}$ = constant. Cylindrical polar coordinates are used.

4.1 MAIN ASSUMPTIONS. — *a*) The whole process is stationary : we will not attempt to describe transient phenomena.

b) T, $\mathbf{V}$, and $\mathbf{n}$ depend only on r and Z.

c) The z dependence of T will be neglected : $T = T(r)$. This is allowed because the thickness of the droplet is small. Therefore any z variation of T will be quickly smeared out by thermal diffusion.

d) Only z derivatives of $\mathbf{v}$ and $\mathbf{n}$ will be considered since the boundary conditions at $Z = 0$ and $Z = Z_0$ impose a strong variation of $\mathbf{v}$ and $\mathbf{n}$ along Z. For instance, $\mathbf{v}$ reaches its maximum at Z_0, as will be shown later

$$\left| \frac{\partial \mathbf{v}}{\partial Z} \right| \gg \left| \frac{\partial \mathbf{v}}{\partial r} \right|$$

$$\left| \frac{\partial \mathbf{n}}{\partial Z} \right| \gg \left| \frac{\partial \mathbf{n}}{\partial r} \right| .$$

e) We make the one-constant approximation [12] for the elastic coefficients and the heat conductivity and replace their tensor value by some average scalar value $\bar{K}$ and $\bar{\kappa}$.

f) We restrict ourselves to deformations of the shape of the drop which are small compared to its thickness.

g) We consider only distances r to the hot spot much greater than the droplet thickness, $r \gg Z_0$. Moreover, we cannot hope to describe in detail what happens in the neighbourhood of the singular line OP of figure 3.

4.2 TEMPERATURE DISTRIBUTION. — Recalling that the temperature distribution T is function of r only, the equation for T in cylindrical coordinates is written

$$\Delta T = \frac{\mathrm{d}^2 T}{\mathrm{d}r^2} + \frac{1}{r}\frac{\mathrm{d}T}{\mathrm{d}r} \equiv 0$$

where Δ is the Laplace operator. Convective terms have been neglected here. This will be shown to be valid for our experimental conditions in section 5.4. Therefore

$$\frac{\mathrm{d}T}{\mathrm{d}r} = \frac{T_0}{r} \qquad (1)$$

T_0 being some constant. Writing that the heat power q generated at the hot point is balanced by the heat losses due to thermal conduction across any cylindrical section of the droplet, one gets easily

$$\frac{\mathrm{d}T}{\mathrm{d}r} = \frac{q}{2\,\pi\bar{\kappa} z_0\, r} . \qquad (2)$$

Thus the temperature decreases logarithmically with the distance r to the heating spot.

4.3 VELOCITY DISTRIBUTION. — To determine the velocity field, we will follow the method of Landau and Lifshitz [15]. At this stage, we will neglect the slight corrections to the velocity due to the local molecular orientation and consider the fluid as isotropic with an average viscosity $\bar{\eta}$. Taking the velocity field to be radial, as observed experimentally, we get :

$$V_r(r, Z) = u(r)\, f(Z/Z_0)\,. \tag{3}$$

The pressure in the layer is given by :

$$P(r, Z) = P_0 + \rho g[Z_0(r) - Z]$$

P_0 is the external pressure acting on the free surface. Notice that Z_0 depends on r. The temperature variation of the density ρ has been neglected ([2]).

The Navier-Stokes equation is :

$$-\eta \frac{\partial^2 V_r}{\partial Z^2} = \frac{\partial P}{\partial r} = g\rho \frac{\mathrm{d}Z_0}{\partial r}\,. \tag{4}$$

This last equation has to be solved with the boundary conditions

$$\sigma^V_{rZ}(h) = \bar{\eta}\left(\frac{\partial V_r}{\partial Z} + \frac{\partial V_Z}{\partial r}\right)_{z=h} \cong$$

$$\cong \eta \frac{-\partial V_r}{\partial Z} = \frac{\mathrm{d}\sigma}{\mathrm{d}r} = \frac{\mathrm{d}\sigma}{\mathrm{d}T} \cdot \frac{\mathrm{d}T}{\mathrm{d}r}$$

$$V_r(0) = 0$$

σ^V_{rz} is here the viscous stress tensor. If the process is stationary, we must include the condition that there is no net flow through a cylindrical section r = constant :

$$\int_0^{Z_0} V\,\mathrm{d}Z = 0$$

(4) is then easily integrated and yields

$$V_r = \frac{3 Z_0}{2\bar{\eta}} \frac{\mathrm{d}\sigma}{\mathrm{d}T} \cdot \frac{\mathrm{d}T}{\mathrm{d}r} \left[\frac{\tilde{Z}^2}{2} - \frac{\tilde{Z}}{3}\right] =$$

$$= \frac{-3 \dfrac{\mathrm{d}\sigma}{\mathrm{d}T} q}{4\pi\kappa\bar{\eta}} \cdot \frac{\dfrac{\tilde{Z}^2}{2} - \dfrac{\tilde{Z}}{3}}{r} \tag{5}$$

([2]) This omission is allowed if

$$\left| \frac{\dfrac{\mathrm{d}\rho}{\mathrm{d}T} g z_0^2}{\dfrac{\mathrm{d}\sigma}{\mathrm{d}T}} \right| \ll 1\,.$$

In our case, this ratio is approximately 10^{-3}.

where

$$\tilde{Z} = \frac{Z}{Z_0}\,.$$

Comparison with (3) yields

$$u(r) = \frac{3 \dfrac{\mathrm{d}\sigma}{\mathrm{d}T}}{4\pi\kappa\bar{\eta}} \frac{q}{r}\,; \qquad f(\tilde{Z}) = \frac{\tilde{Z}^2}{2} - \frac{\tilde{Z}}{3}\,. \tag{6}$$

Thus V depends on both r and Z ; V is maximum on the free surface $\tilde{Z} = 1$.

4.4 EQUILIBRIUM CONDITIONS FOR THE DIRECTOR FIELD. — The coupling between the velocity field **V** and the director field **n** is a well known property of liquid crystals and has been reviewed recently [12]. In this problem, the initial molecular orientation will be distorted by the hydrodynamic flow created by the thermally-induced surface tension change in the droplet. The director field $\mathbf{n}(r, z)$ is described by two angles θ and φ, which, on the surface, take the values θ_s and φ_s. θ is the tilt angle between **n** and the horizontal plane and φ is the azimuthal angle between the horizontal projection of **n** and the **OX** axis (see Fig. 1).

The boundary conditions for θ and φ are :

$$\varphi = 0\,, \qquad \theta = 0 \quad \text{at} \quad Z = 0 \tag{7a}$$

$$\frac{\partial \varphi}{\partial Z} = 0\,, \qquad \theta = \theta_s \quad \text{at} \quad Z = Z_0 \tag{7b}$$

(7*b*) is typical for a free surface ; we assume (7*b*) to be true, even if Z_0 depends slightly on r.

One now writes that, at equilibrium, the total torque due to the elastic and hydrodynamic forces acting on **n** vanishes

$$\boldsymbol{\Gamma}^{\mathrm{tot}} = \boldsymbol{\Gamma}_{\mathrm{el}} + \boldsymbol{\Gamma}_{\mathrm{v}} \tag{8}$$

where the elastic torque $\boldsymbol{\Gamma}_{\mathrm{el}}$ and the viscous torque $\boldsymbol{\Gamma}_{\mathrm{v}}$ are given by :

$$\boldsymbol{\Gamma}_{\mathrm{el}} = \mathbf{n} \wedge \bar{K}\,\Delta\mathbf{n}$$

$$\boldsymbol{\Gamma}_{\mathrm{v}} = -\,\mathbf{n} \wedge [(\alpha_3 - \alpha_2)\,\mathbf{N} + (\alpha_2 + \alpha_3)\,\hat{A}\mathbf{n}]\,.$$

Under stationary conditions, N_i is equal to $\Omega_{ij}\, n_j$; $\hat{A}\mathbf{n}$ is a vector with components $A_{ij}\, n_j$. The matrices A_{ij} and Ω_{ij} represent the symmetric and antisymmetric part respectively of the velocity derivative tensor $\partial_i V_j$ whose unique non-vanishing term here is $\partial_Z V_r$. α_2 and α_3 are Leslie coefficients [16].

Because of the special shape of $\boldsymbol{\Gamma}_{\mathrm{el}}$ and $\boldsymbol{\Gamma}_{\mathrm{v}}$, equation (8) can be split into two independent equations only, corresponding to the r — and z — components of $\boldsymbol{\Gamma}_{\mathrm{tot}}$, respectively.

Using

$$\beta = \psi - \varphi$$

$$\mathbf{n} = (\cos\theta \cos\beta,\ -\cos\theta \sin\beta,\ \sin\theta)$$

(see Fig. 4) and noticing that :

$$\Gamma_{\text{el},\alpha} = \bar{K}\left(n_\beta \frac{\partial^2 n_\gamma}{\partial Z^2} - n_\gamma \frac{\partial^2 n_\beta}{\partial Z^2}\right) = \frac{\partial}{\partial Z}\left[\bar{K}\left(n_\beta \frac{\partial n_\gamma}{\partial Z} - n_\gamma \frac{\partial n_\beta}{\partial Z}\right)\right].$$

(α, β, γ = even permutation of r, ψ, Z).

One gets easily :

$$\Gamma_{\text{tot}\,r} = \bar{K}\frac{\mathrm{d}}{\mathrm{d}Z}\left(-\sin\beta\frac{\mathrm{d}\theta}{\mathrm{d}Z} + \sin\theta\cos\theta\cos\beta\frac{\mathrm{d}\beta}{\mathrm{d}Z}\right) + \alpha_3\,\partial_Z V_r \cos^2\theta\cos\beta\sin\beta = 0 \tag{9a}$$

$$\Gamma_{\text{tot}\,Z} = \bar{K}\frac{\mathrm{d}}{\mathrm{d}Z}\left(-\cos^2\theta\frac{\mathrm{d}\beta}{\mathrm{d}Z}\right) - \alpha_2\,\partial_Z V_r \sin\theta\cos\theta\sin\beta = 0 \tag{9b}$$

with the boundary conditions

$$\left.\begin{aligned} &\theta = 0\,, \quad \beta = \psi \quad \text{for} \quad Z = 0 \\ &\theta = \theta_s\,, \quad \frac{\mathrm{d}\beta}{\mathrm{d}Z} = 0 \quad \text{for} \quad Z = Z_0 \end{aligned}\right\}. \tag{10}$$

We are interested mainly in the value of φ_s on the surface. At this stage, we can get much information from very simple considerations ; we shall postpone a more detailed treatment of equation (9) to the appendix. The behaviour of φ_s is mainly described by equation (9*b*), i.e. by the vertical component of the total torque (see appendix). The shear gradients are essentially concentrated in the neighbourhood of the surface ; therefore, we can estimate the order of magnitude of both terms in (9*b*).

Noticing first that :

$$\frac{\mathrm{d}^2\beta}{\mathrm{d}Z^2} = -\frac{\mathrm{d}^2\varphi}{\mathrm{d}Z^2} \sim -\frac{\varphi_s}{Z_0^2}$$

and replacing the different functions by their value at $Z = Z_0$. We get

$$\bar{K}\frac{\varphi_s}{Z_0^2} \approx -\alpha_2\frac{u(r)}{Z_0}\sin(\psi - \varphi_s)\,. \tag{11}$$

The term on the left-hand side of (11) represents a restoring torque proportional to φ_s ; the right-hand side describes the viscous torque due to the velocity field. It depends on the sine of the angle $\psi - \varphi_s$ between **n** and **v** (recall that $\alpha_2 < 0$) (16).

Using (5), one rewrites (11) in the form :

$$\varphi_s = \frac{r_0}{r}\sin(\psi - \varphi_s)\,. \tag{12}$$

A more careful treatment of (9) shows that (12) is the first-step solution of a self-consistent resolution procedure of (9) (see appendix). Moreover, the calculation gives a numerical value for the characteristic length r_0 appearing in (12). One gets :

$$r_0 = \frac{5\left|\alpha_2\frac{\mathrm{d}\sigma}{\mathrm{d}T}\right| q\theta_s Z_0}{48\,\pi\overline{K\kappa\eta}} \tag{13}$$

when neglecting corrections of the order θ_s^3.

It is striking that the distortion associated with the flow exists only if $\theta_s \neq 0$. If the molecules lay flat on the surface ($\theta_s = 0$) equations (12) and (13) show that $\varphi_s \equiv 0$. (Only in the limits of the approximation which leads to the equations (11) or (12).)

Using this value of the characteristic length of the problem, we can rewrite the velocity field (5) as :

$$V_r(r, Z) = V_0\frac{r_0}{r}\frac{Z}{Z_0}\left(3\frac{Z}{Z_0} - 2\right) \tag{14}$$

V_0, the value of velocity at $r = r_0$ and $Z = Z_0$ is given by :

$$V_0 = \frac{6}{5}\frac{\bar{K}}{(-\alpha_2)\,\theta_s\,Z_0}\,.$$

4.5 DESCRIPTION OF THE MOLECULAR ORIENTATION ON THE FREE SURFACE. — The molecular orientation at the nematic-air interface is described by the two angles φ_s and θ_s (Fig. 1).

We have already shown in 4.4 that φ_s satisfies equation (12)

$$\varphi_s = \frac{r_0}{r}\sin(\psi - \varphi_s) \tag{12}$$

θ_s is taken to be a constant since the anchoring conditions for the tilt angle are assumed to be strong. In fact, careful experiments [1] shown that θ_s is insensitive to strong external fields.

Numerical solutions of equation (12) are displayed graphically on figure 5 as the projection of the molecular orientation onto the free surface. Our theoretical model gives a distorted configuration with a disconti-

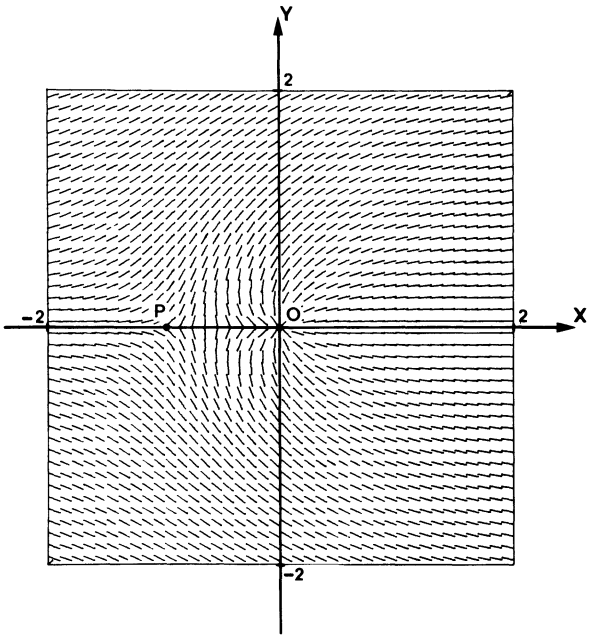

FIG. 5. — Numerical calculation of the distorted molecular orientation on the free surface.

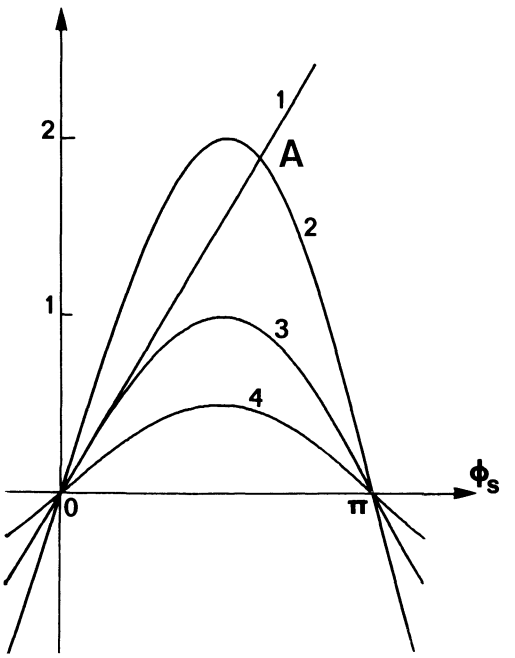

FIG. 6. — Solutions of equation (12) $\varphi_s = r_0/r \sin(\psi - \varphi_s)$ are given by the intersections of the curve $f = \varphi_s$ with the curve $f = r_0/r \sin(\psi - \varphi_s)$. It is particularly interesting to study the case $\psi = \pi$, which corresponds to the direction of the singular line **OP**. 1) At a distance $r = r_0/2$ ($r_0 = |\mathbf{OP}|$) from the hot spot (0) there is a non-vanishing distortion φ_s (see also Fig. 5) corresponding to the graphical solution (point A) of the equation $f(2) = 2 \sin(\pi - \varphi_s) = \varphi_s$ (or more precisely there is a pair of solutions φ_s and $-\varphi_s$, which are obtained when approaching the OP line from above or below respectively). The distortion angle φ_s goes continuously to zero when approaching the singular point P($r = r_0$). 2) At $r = r_0$ the solution of the equation

$$f(3) = \sin(\pi - \varphi_s) = \varphi_s$$

is $\varphi_s = 0$. 3) Outside the region of the singular line OP (for $r > r_0$) there is no distortion; for example for $r = 2\,r_0$ the equation $f(4) = \frac{1}{2} \sin(\pi - \varphi_s) = \varphi_s$ has only one solution, namely $\varphi_s = 0$.

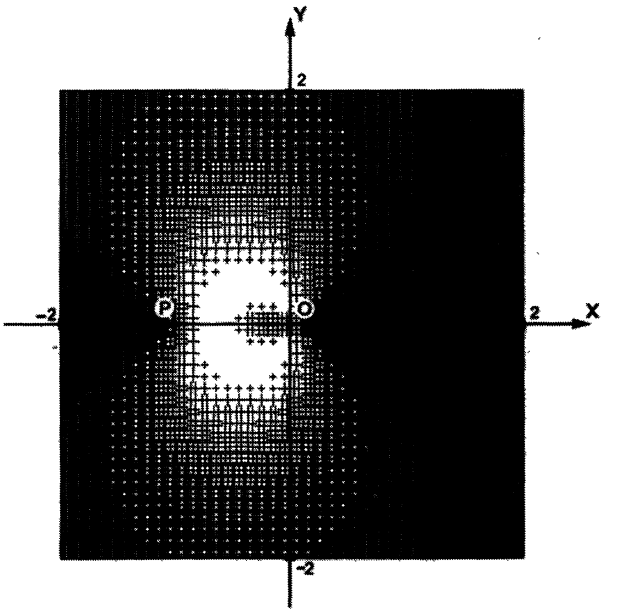

FIG. 7. — Numerical calculation of the transmitted intensity between crossed polarizers following the laser heating.

nuity line terminated by 2 singular points O and P. Its length is r_0 as can be demonstrated with a simple graphic argument given in figure 6.

It is also interesting to simulate the light intensity transmitted between crossed polarizers to allow for a straightforward comparison with our experimental results. This is done in figure 7.

5. **Comparison with experiment.** — We shall compare here the main predictions of the theory with our experimental results, namely the general structure of the director field on the free surface, the distance between the two singular points O and P, and the dependence of the molecular distortion on the anchoring conditions.

5.1 MOLECULAR ORIENTATION ON THE FREE SURFACE. — In the initial state, the local optical axis is uniform throughout the surface.

In the distorted state, the theoretical model predicts a deformation of the molecular orientation which is continuous everywhere, except for one discontinuity line between two singular points.

The observation of the light intensity transmitted by the sample between crossed polarizers is in agreement with this model. Figure 2 shows a striking similarity with the calculated intensity pattern of figure 7.

Therefore, it is reasonable to assume that the molecular configuration on the free surface is correctly described by our model picture of figure 5. At this point, it should be noticed that our model breaks down close to the director field singularities since only long range order distortions were taken into account.

In fact, the singular line predicted by the theory is more like a narrow wall than a true discontinuity, since continuous changes of the molecular alignment are energetically more favourable.

5.2 DISTANCE BETWEEN THE TWO SINGULAR POINTS 0 AND P. — The distance r_0 between the two singular points O and P is given by equation (13). r_0 gives the scale length of the molecular distortion. Following equation (13), r_0 is expected to be proportional to the heating power q. This linear dependence is indeed observed experimentally as shown in figure 3 where r_0 is plotted as a function of the incident laser power.

A more quantitative comparison between the theoretical and experimental values of r_0 is possible. Taking $\alpha_2 = -0.7\ p$ [16], $d\sigma/dT = -0.1$ dyne/cm °C [1], $\overline{K} = 10^{-6}$ dyne [12], $\overline{\eta} = 0.5\,p$ [12], $\theta_s = 15°$ [3], from the literature, and $dT/dr = 1.7°$/cm for $r = 500$ μm and $Z_0 = 100$ μm from our experimental conditions, we get $r_0 = 600$ μm.

This has to be compared with our observed value of 500 μm. The agreement is reasonable. A greater accuracy cannot be expected in view of the crudeness of our theoretical approximations and of the number of parameters involved.

5.3 DEPENDENCE OF THE MOLECULAR DISTORTION ON THE ANCHORING CONDITIONS. — It is obvious from equations (12) and (13) that the molecular distortion induced by the hydrodynamic flow is strongly dependent on the molecular tilt angle on the free surface. In particular, the initial configuration will stay undistorted in a first approximation if θ_s is zero.

This point has been checked in separate experiments on the nematic P.A.A. (p-azoxyanisol), in which the molecules are known to align parallel to the free surface [17]. In this case, no molecular distortion was observed whatever the heating power, although hydrodynamic flows were clearly present. The explanation is obvious if we notice that in this geometry, the initial hydrodynamic torque is proportional to α_3, instead of α_2 as in the case where θ_s is non zero. As α_3 is much smaller than α_2, the molecular distortion is too weak to be observable under the same experimental conditions previously used for MBBA.

5.4 SURFACE TENSION AGAINST GRAVITATION FORCES. — In principle one should also consider the action of buocyancy forces to explain the temperature-induced fluid motion within the droplet. However, we believe that these forces can be neglected here and that only surface tension forces have to be considered. This is most easily demonstrated by turning the glass plate supporting the droplet upside down and by repeating the same experiment. The flow circulation is reversed. On the contrary, were the gravitation forces predominant, flow motion should have not reversed.

Also it should be emphasized that the calculations of the temperature distribution have assumed that heat convection can be neglected this is only if the thermal diffusion time t_D is always much smaller than the characteristic thermal convection time t_c

$$t_D = r^2/D\,, \qquad t_c = r/v$$

where D is the thermal diffusivity ($\sim 10^{-4}$ c.g.s. [18]) and v the local velocity at the distance r from the heating point.

The ratio t_D/t_c is indeed much less than 1. Noticing that this ratio is independent of r, since equation (5) shows that the product vr is a constant, we get $t_D/t_c \simeq 10^{-1}$, using $v \sim 20$ μm/s at $r = 500$ μm from our experimental observations.

6. **Conclusions.** — In the stationary regime, the situation seems relatively clear. The local temperature heating induces changes in surface tension which in turn create hydrodynamic flows. Depending on the molecular orientation on the free surface, this streaming can distort the initial director field. Our theoretical treatment is in reasonable agreement with the observations. The overall structure of the distorted molecular orientation has been well understood. However, the large number of parameters involved in the problem (surface tension, thermal gradients, anisotropic viscosities, elastic coefficients, etc.) makes quantitative determination very difficult. At any rate, this effect can certainly be used as an easy method of discrimination between a zero and a finite molecular tilt angle on the free surface, which has been a matter of controversy for a long time.

All our observations were made around room temperature. Interesting phenomena could also be observed in the temperature region where $d\sigma/dT$ changes sign [2]. The streaming effect should disappear when $d\sigma/dT = 0$. When $d\sigma/dT$ is positive, one expects a sign reversal of the hydrodynamic flow and the observed intensity pattern should be the mirror image of the present case.

Possible extensions of this work would be to study non-stationary regimes and also to investigate other possible geometries in various liquid crystalline phases.

Acknowledgments. — We gratefully acknowledge helpful discussions with E. Guyon and E. Dubois-Violette. The M.B.B.A. and the dye were kindly supplied to us by L. Streczlecki and L. Liebert at the Université de Paris-Sud, Orsay.

Appendix. — Analysis of the equilibrium conditions.

We have to consider equations (9)

$$\frac{\mathrm{d}}{\mathrm{d}Z}\left(-\sin\beta\frac{\mathrm{d}\theta}{\mathrm{d}\tilde{Z}}+\sin\theta\cos\theta\cos\beta\frac{\mathrm{d}\beta}{\mathrm{d}\tilde{Z}}\right)-E_{r_3}\left(\tilde{Z}-\frac{1}{3}\right)\cos^2\theta\cos\beta\sin\beta=0 \qquad \text{(A1.}a\text{)}$$

$$\frac{\mathrm{d}}{\mathrm{d}\tilde{Z}}\left[-\cos^2\theta\frac{\mathrm{d}\beta}{\mathrm{d}\tilde{Z}}\right]+E_{r_2}\left(\tilde{Z}-\frac{1}{3}\right)\sin\theta\cos\theta\sin\beta=0 \qquad \text{(A1.}b\text{)}$$

which have been rewritten here in dimensionless form, where :

$$\tilde{Z}=\frac{Z}{Z_0}$$

$$E_{r_{2,3}}=-\frac{\alpha_{2,3}\,u(r)\,Z_0}{\bar{K}}$$

E_{r_2} and E_{r_3} are r-dependent Ericksen numbers, one for each α_2, α_3. Introducing two functions F and G by the relations

$$F=-\cos^2\theta\frac{\mathrm{d}\beta}{\mathrm{d}\tilde{Z}},\qquad G=-\sin\beta\frac{\mathrm{d}\theta}{\mathrm{d}\tilde{Z}}+\sin\theta\cos\theta\cos\beta\frac{\mathrm{d}\beta}{\mathrm{d}\tilde{Z}}$$

(A1) becomes now :

$$\begin{aligned}
&a)\ \frac{\mathrm{d}\beta}{\mathrm{d}\tilde{Z}}=-\frac{F}{\cos^2\theta}\\
&b)\ \frac{\mathrm{d}\theta}{\mathrm{d}\tilde{Z}}=+F\,\mathrm{tg}\,\theta\,\mathrm{cotg}\,\beta-\frac{G}{\sin\beta}\\
&c)\ \frac{\mathrm{d}F}{\mathrm{d}\tilde{Z}}=-E_{r_2}\sin\theta\cos\theta\sin\beta\left(\tilde{Z}-\frac{1}{3}\right)\\
&d)\ \frac{\mathrm{d}G}{\mathrm{d}y}=E_{r_3}\cos^2\theta\sin\beta\cos\beta\left(\tilde{Z}-\frac{1}{3}\right)
\end{aligned} \qquad \text{(A2)}$$

with the boundary conditions, deduced from (10) :

$$\begin{aligned}
&\theta=0\,,\qquad \beta=\psi \qquad \text{for} \qquad \tilde{Z}=0\\
&\theta=\theta_s\,,\qquad F=0 \qquad \text{for} \qquad \tilde{Z}=1\,.
\end{aligned} \qquad \text{(A3)}$$

In order to obtain the value φ_s of φ on the surface, we formally integrate (A2.a) by parts ; using (A2.c) and (A3) ; we then get :

$$\begin{aligned}
\varphi_s&=-(\beta(1)-\beta(0))=\int_0^1\mathrm{d}\tilde{Z}\frac{F}{\cos^2\theta}\\
&=E_{r_2}\int_0^1\mathrm{d}\tilde{Z}\sin\theta\cos\theta\left(\tilde{Z}-\frac{1}{3}\right)\sin(\psi-\varphi)\int_0^{\tilde{Z}}\frac{\mathrm{d}\tilde{Z}}{\cos^2\theta}\,.
\end{aligned} \qquad \text{(A4)}$$

At very large distances from the hot point ($r=0$), E_{r_2} and E_{r_3} vanish ; (A2) and (A3) then yield the obvious solution

$$\theta \quad \text{''} \quad \varphi=0\,. \qquad \text{(A5)}$$

Therefore, for large values of r, the actual solution of (A2) differs from (A5) by corrections of order E_r. We first replace θ in (A4) by its value (A5). In the right hand side of this last equation, sin $(\psi-\varphi)$ is now multiplied by a factor which is a strongly increasing function of $\tilde{Z}$ between 0 and 1 ; moreover, φ is stationary for $\tilde{Z}=1$ (its first derivative vanishes there).

We therefore replace φ by φ_s in (A4) and get :

$$\varphi_s = \sin(\psi - \varphi_s) E_{r_2} \int_0^1 d\tilde{Z} \sin\theta_s \tilde{Z} \cos\theta_s \tilde{Z} \left(\tilde{Z} - \frac{1}{3}\right) \int_0^z \frac{d\tilde{Z}}{\cos^2\theta_s \tilde{Z}}.$$

The computation of Γ_0 is then elementary and yields (13) in the limit $\theta_s \to 0$.

References

[1] LANGEVIN, D., *J. Physique* **33** (1972) 249.

[2] KRISHNASWAMY, S. and SHASHIDAR, R., *Mol. Cryst. Liq. Cryst.* **35** (1976) 253.

[3] BOUCHIAT, M. A. and LANGEVIN, D., *Phys. Lett.* **34** (1971) 331.

[4] PROST, J. and GASPAROUX, H., *C. R. Hebd. Séan. Acad. Sci.* **271B** (1971) 1076.

[5] VILANOVE, R., GUYON, E., MITESCU, C. and PIERANSKI, P., *J. Physique* **35** (1974) 153.

[6] PARSONS, J. D., *J. Physique* **37** (1976) 1187.

[7] BIKERMAN, J. J., *Surface Chemistry* 2nd ed. (Academic Press, New York) 1958.
PEARSON, J. R. A., *J. Fluid Mech.* **4** (1958) 489.

[8] BÉNARD, H., *Ann. Chim. Phys.* **23** (1901) 62.

[9] GRODZKA, P. G. and BANNISTER, T. C., *Science* **187** (1975) 165.

[10] ANDERSSON, D., *J. Colloid Interface Sci.* **56** (1976) 184.

[11] JANNING, J. L., *Appl. Phys. Lett.* **21** (1973) 173.

[12] DE GENNES, P. G., *The physics of liquid crystals* (Oxford Press) 1974.

[13] RONDELEZ, F., *Philips Res. Rep. Suppl.* **2** (1974) 1.

[14] MAUGUIN, C., *Bull. Soc. Fr. Mineral. Cristallogr.* **34** (1911) 3, see also Ref. [12].

[15] LANDAU, L. and LIFSHITZ, E., *Physique Théorique VI, Mécanique des Fluides*, p. 296 (Editions Mir) Moscou, 1971.

[16] GÄHWILLER, Ch., *Phys. Lett.* **36A** (1971) 311.

[17] NAGGIAR, V., *C. R. Hebd. Séan. Acad. Sci.* **208** (1939) 1916.

[18] KURODA, S., KIMURA, M. and KUBOTA, K., *Mol. Cryst. Liq. Cryst.* **33** (1976) 235.
URBACH, W., HERVET, H. and RONDELEZ, F., To be published in *Mol. Cryst. Liq. Cryst.*